

Bridge displacement estimation by fusing accelerometer and strain gauge measurements

Zhanxiong Ma | Junyeon Chung | Peipei Liu | Hoon Sohn 

Department of Civil and Environmental Engineering, Korea Advanced Institute of Science and Technology, Daejeon, South Korea

Correspondence

Hoon Sohn, Department of Civil and Environmental Engineering, Korea Advanced Institute of Science and Technology, Daejeon, South Korea.
 Email: hoonsohn@kaist.ac.kr

Funding information

National Research Foundation of Korea (NRF), Grant/Award Number:
 2017R1A5A1014883

Summary

For large-span bridge monitoring, displacement measurement is essential. However, it remains challenging to accurately estimate bridge displacement. When displacement is calculated by the double integration of acceleration, a low-frequency drift appears in the estimated displacement. Displacement can also be estimated from strains based on the Euler–Bernoulli beam theory. However, prior knowledge of the mode shapes and the neutral axis location of the target bridge are required for strain–displacement transformation. In this study, we propose a finite impulse response filter-based displacement estimation technique by fusing strain and acceleration measurements. First, the relationship between displacement and strain is established, and the parameter associated with this strain–displacement transformation is estimated from strain and acceleration measurements using a recursive least squares algorithm. Next, the low-frequency displacement estimated from the strain measurements and the high-frequency displacement obtained from an acceleration measurement are combined for high-fidelity displacement estimation. The feasibility of the proposed technique was examined via a series of numerical simulations, a lab-scale experiment, and a field test. The uniqueness of this study lies in the fact that the displacement and the unknown parameter in strain–displacement transformation are estimated simultaneously and the accuracy of displacement estimation is improved in comparison with those of previous data fusion techniques.

KEY WORDS

accelerometer, data fusion, displacement estimation, finite impulse response filter, strain gauge

1 | INTRODUCTION

Displacement plays a vital role in the monitoring and control of bridge structures as it provides crucial information regarding the structural integrity and condition of the bridges.^{1–4} There are several sensing techniques wherein displacement is directly measured, such as linear variable differential transformer (LVDT),⁵ laser Doppler vibrometer (LDV),⁶ interferometric radar,⁷ real-time kinematic global navigation satellite system (RTK-GNSS),⁸ and vision-based systems.^{9,10} LVDT requires an additional scaffold for operation, making it difficult to apply for large-scale structures. Both LDV and interferometric radar are rather expensive and not applicable for long-term monitoring. RTK-GNSS has

a limited accuracy of around 10 mm, and its sampling rate is only up to 20 Hz. While vision-based system can trace displacement at multiple points, its accuracy is highly affected by light and weather conditions.

Efforts have been made to indirectly estimate displacement from the measurement of the physical quantities related to displacement. For instance, acceleration is most widely used for displacement estimation.^{11–14} When displacement is estimated via the double integration of acceleration, the estimated displacement can have a large, low-frequency drift caused by unknown initial conditions and measurement noises. Although techniques have been suggested to suppress such a low-frequency drift, the techniques often cannot tell the difference between actual structural responses and noise in the same low-frequency band and the low-frequency structural displacement can often be suppressed.^{11,12} Progress has also been made in strain-based displacement estimation techniques,^{15–20} including mode superposition techniques,^{15,16} conjugate beam techniques,^{18,19} and curve fitting technique,²⁰ but all these strain-based techniques have low accuracy owing to their relatively large noise levels.

Data fusion techniques have been proposed for displacement estimation.^{21–25} These techniques combine multiple measurements, such as RTK-GNSS, acceleration, strain, and vision, to produce more accurate displacement estimation. However, the fusion of RTK-GNSS and acceleration does not work under GNSS-denied environments,^{21,22} the fusion of vision and acceleration cannot operate at night,²⁴ and the fusion of strain and acceleration needs to estimate a scale factor for strain–displacement transformation and inaccurate estimation of the scale factor usually deteriorates displacement estimation accuracy.²⁵

In this study, an FIR filter-based displacement estimation technique is proposed for bridge structures by fusing strain and acceleration measurements, and the proposed technique can estimate displacement with high accuracy even in GNSS-denied conditions and dark areas. First, pure bending strains are extracted from strain measurements and then transformed into displacement. Here, the mode shapes from a uniform simply supported beam, called assumed mode shapes hereafter, are used in strain–displacement transformation, and a scale factor is included to compensate the discrepancies between the assumed and true mode shapes. The value of the scale factor is estimated from the strain and acceleration measurements using a recursive least squares (RLS) algorithm.²⁶ Then, the low-frequency displacement estimated from the strain measurements and the high-frequency displacement obtained from an acceleration measurement are combined using the FIR filter for high-fidelity displacement estimation. The uniqueness of this study lies in that (1) displacement can be estimated using strain and acceleration measured with different sampling rates, (2) displacement and the unknown scale factor are estimated simultaneously, and (3) the accuracy of displacement estimation is improved in comparison with those of previous data fusion techniques.

The paper is organized as follows. The proposed displacement estimation technique is formulated in Section 2. In Section 3, the performance of the proposed technique is examined using numerical simulations of simply supported beam models, and the effects of number and locations of strain gauges on displacement estimation accuracy are investigated. In Section 4, a series of numerical simulations are conducted using beam models to demonstrate that the scale factor can effectively compensate the error caused by the discrepancies between the assumed and true mode shapes. In Section 5, an FE model of Jindo Grand Bridge in South Korea is used to validate the proposed technique by extracting pure bending strains from strain measurements. Experimental validation using a fixed-fixed beam specimen and a pedestrian bridge is provided in Section 6. The concluding remarks are given in Section 7.

2 | DEVELOPMENT OF FIR FILTER-BASED DISPLACEMENT ESTIMATION TECHNIQUE

In this section, a displacement estimation technique using strain and acceleration measurements is developed. The overview of the proposed technique is shown in Figure 1. First, strain measurements from multiple strain gauges are

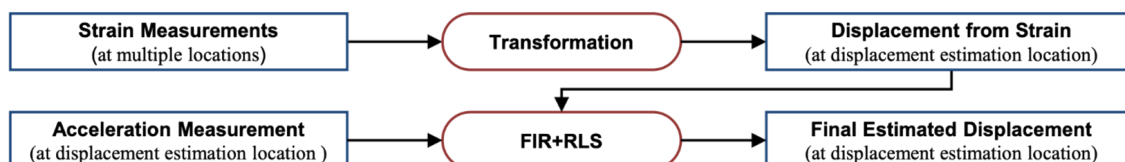


FIGURE 1 Overview of the proposed displacement estimation technique

transformed into the displacement. Because strain gauges usually have large noises, the transformed displacement has low accuracy. An accelerometer is placed at the location where displacement needs to be estimated. Then, the acceleration measurement and the transformed displacement from strain measurements are combined using an FIR filter and an RLS algorithm.

2.1 | Strain-displacement transformation

A mode-based technique has been proposed to transform strain measurements into displacement.¹⁵ This technique assumes that the bridge has a uniform cross-section and the measured strains are mainly due to bending. In reality, most bridges have varying cross-sections and the strain measurement comprises pure bending and axial strains. In this section, a strain-displacement transformation equation is established for bridges with varying cross-sections by extracting pure bending strain from strain measurements. Note that the static displacement caused by dead loads such as gravity and prestressing is not considered here since strain sensors will be installed after the complete of the bridge.

An Euler-Bernoulli beam model with varying cross-sections and subjected to vertical and axial loadings are shown in Figure 2. Here, the strain at an arbitrary cross-section, $\varepsilon(x, y, k)$, can be decomposed into uniform axial strain, $\varepsilon^u(x, k)$, and linearly varying bending strain, $\varepsilon^b(x, y, k)$, as shown in Figure 3.²⁷

$$\varepsilon(x, y, k) = \varepsilon^u(x, k) + \varepsilon^b(x, y, k), \quad (1)$$

where k represents the k th time step.

From the bending strain, the strain-displacement relationship can be express as

$$\varepsilon^b(x, y, k) = y \frac{d^2 u(x, k)}{dx^2}, \quad (2)$$

where u is the vertical (y -directional) displacement of the beam. Assuming that two strain gauges are placed at different heights of the cross-section, the relationship between the difference of the strains from two strain gauges, $\Delta\varepsilon$, and displacement is obtained as follows:

$$\Delta\varepsilon(x, k) = h(x) \frac{d^2 u(x, k)}{dx^2}, \quad (3)$$

where $h(x)$ is the vertical distance between two strain gauges.

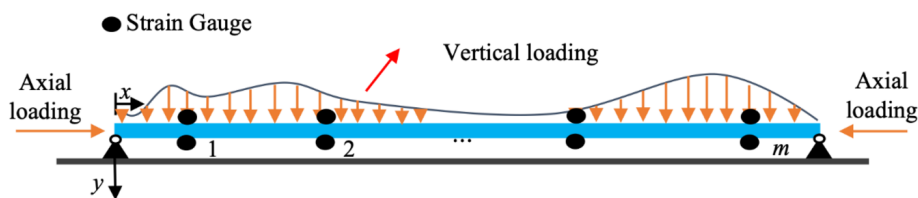


FIGURE 2 Euler–Bernoulli beam subjected to both vertical and axial loadings

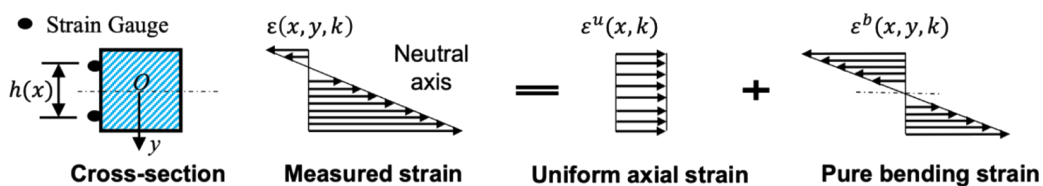


FIGURE 3 Decomposition of strain across the beam cross-section into uniform axial strain and pure bending strain

According to a modal superposition method, $u(x, k)$ can be expressed as follows:

$$u(x, k) = \sum_{j=1}^L \varphi_j(x) q_j(k), \quad (4)$$

where φ_j represents the j th mode shape, q_j represents the j th modal response, and L is the number of modes considered. Substituting Equation 4 into Equation 3, $\Delta\epsilon(x, k)$ can also be expressed as the superposition of the modal responses.

$$\Delta\epsilon(x, k) = h(x) \sum_{j=1}^L \frac{d^2\varphi_j(x)}{dx^2} q_j(k). \quad (5)$$

Supposing that the strains are measured at multiple points ($x = x_i$, $i = 1, \dots, m$), Equation 5 can be rewritten in a matrix form

$$\Delta\boldsymbol{\epsilon}(k) = \mathbf{H}\Phi\mathbf{q}(k), \quad (6)$$

where

$$\Delta\boldsymbol{\epsilon}(k) = [\Delta\epsilon(x_1, k) \dots \Delta\epsilon(x_m, k)]_{1 \times m}^T, \quad (7)$$

$$\mathbf{q}(k) = [q_1(k) \dots q_L(k)]_{1 \times L}^T, \quad (8)$$

$$\Phi = \begin{bmatrix} \frac{d^2\varphi_1(x_1)}{dx^2} & \dots & \frac{d^2\varphi_L(x_1)}{dx^2} \\ \vdots & \ddots & \vdots \\ \frac{d^2\varphi_1(x_m)}{dx^2} & \dots & \frac{d^2\varphi_L(x_m)}{dx^2} \end{bmatrix}_{m \times L}, \quad (9)$$

$$\mathbf{H} = \begin{bmatrix} h(x_1) & \dots & 0 \\ \vdots & \ddots & \vdots \\ 0 & \dots & h(x_m) \end{bmatrix}_{m \times m}. \quad (10)$$

Then, the modal responses $\mathbf{q}(k)$ can be estimated from Equation 6.

$$\mathbf{q}(k) = (\Phi^T \Phi)^{-1} \Phi^T \mathbf{H}^{-1} \Delta\boldsymbol{\epsilon}(k). \quad (11)$$

Note that the number of strain measurement points, m , should be equal to or larger than the number of modes considered, L , to avoid rank deficiency of the matrix Φ . Introducing Equation 11 into Equation 4, the displacement at any location $x = x_d$ can be represented as

$$u(k) = \mathbf{T}\mathbf{H}^{-1} \Delta\boldsymbol{\epsilon}(k), \quad (12)$$

where

$$\mathbf{T} = \Psi(x_d) [\Phi^T \Phi]^{-1} \Phi^T, \quad (13)$$

$$\Psi = [\varphi_1(x_d) \dots \varphi_L(x_d)]_{1 \times L}. \quad (14)$$

To estimate displacement from strain measurement using Equation 12, a prior knowledge of the mode shapes is required. In this study, the mode shapes from a simply-supported beam with a uniform cross-section is used to approximate matrix \mathbf{T} . When a numerical model of the bridge is available, the mode shapes obtained from the numerical model can also be used instead of the ones obtained from the simply supported beam to approximate matrix \mathbf{T} . Then, a scale factor α is introduced to compensate for the differences between the assumed mode shapes and true ones:

$$\mathbf{u}(k) = \frac{1}{\alpha(k)} \mathbf{T}_a \mathbf{H}^{-1} \Delta \boldsymbol{\epsilon}(k). \quad (15)$$

Note that \mathbf{T}_a is the approximation of matrix \mathbf{T} . An RLS algorithm is developed in Section 2.3 to estimate the scale factor α from the strain and acceleration measurements.

2.2 | Introduction to FIR filter-based displacement estimation

Lee et al. proposed an FIR filter-based technique to estimate displacement from acceleration measurement,¹¹ and this technique has been extended to allow for the fusion of acceleration and strain measurements for improved displacement estimation.²⁵ For the completeness of the study, the basic principle is summarized below. Note that it is assumed that strain and acceleration are measured with the same sampling rate.

Provided that acceleration measurement and displacement estimation from strain measurements are available, an error function $\Pi\{\mathbf{u}^*\}$ is defined within a given time window $[(k - N)\Delta t, (k + N)\Delta t]$ as follows:

$$\Pi(\mathbf{u}^*) = \frac{1}{2} \|\mathbf{L}_a \mathbf{L}_c \mathbf{u}^* - \mathbf{L}_a (\Delta t)^2 \mathbf{a}\|_2^2 + \frac{\lambda^2}{2} \|\mathbf{u}^* - \mathbf{u}\|_2^2, \quad (16)$$

where \mathbf{u}^* , \mathbf{u} , and \mathbf{a} are the final displacement estimation vector $[u^*(k - N), u^*(k - N + 1), \dots, u^*(k + N)]^T$, vector of the displacement transformed from strain measurements $[u(k - N), u(k - N + 1), \dots, u(k + N)]^T$, and measured acceleration vector $[a(k - N + 1), a(k - N + 2), \dots, a(k + N - 1)]^T$, respectively. Δt is the time interval of measurements. $\|\cdot\|_2$ denotes the two-norm of a vector, \mathbf{L}_a is a diagonal weighting matrix of the order $(2N - 1)$ with all diagonal entries being 1 except the first and last entries, which are equal to $1/\sqrt{2}$, \mathbf{L}_c is the second-order differential operator matrix based on the discretized trapezoidal rule, and λ is the regularization factor defined as

$$\lambda = 46.81(2N + 1)^{-1.95}, \quad (17)$$

where $(2N + 1)$ is the number of time steps within the time window and is suggested to be

$$2N + 1 = \frac{2.68}{f_1 \Delta t}, \quad (18)$$

where f_1 is the first natural frequency of the target structure. More details can be found in Lee et al.¹¹

Then, the final displacement estimation can be obtained by minimizing the error function $\Pi\{\mathbf{u}^*\}$ with respect to \mathbf{u}^* , and the least squares solution is given as

$$\mathbf{u}^* = (\Delta t)^2 (\mathbf{L}^T \mathbf{L} + \lambda^2 \mathbf{I})^{-1} \mathbf{L}^T \mathbf{L}_a \mathbf{a} + \lambda^2 (\mathbf{L}^T \mathbf{L} + \lambda^2 \mathbf{I})^{-1} \mathbf{u}, \quad (19)$$

where \mathbf{L} is $\mathbf{L}_a \mathbf{L}_c$. Although the displacement at each time step within the time window can be estimated using Equation 19, the accuracy is highest at the center of the time window. Thus, an overlapping moving window technique is adopted, and only the displacement estimated at the center of each time window is retained.

$$u^*(k) = \mathbf{C}_H \mathbf{a} + \mathbf{C}_L \mathbf{u}, \quad (20)$$

where \mathbf{C}_H is the $(N + 1)$ th row of the matrix $\{(\Delta t)^2(\mathbf{L}^T \mathbf{L} + \lambda^2 \mathbf{I})^{-1} \mathbf{L}^T \mathbf{L}_a\}$ and is a combination of a double integrator and a high-pass filter. \mathbf{C}_L is the $(N + 1)$ th row of the matrix $\{\lambda^2(\mathbf{L}^T \mathbf{L} + \lambda^2 \mathbf{I})^{-1}\}$ and is a low-pass filter.¹¹

It must be noted that aforementioned FIR filter cannot be directly applied to estimate displacement using strain and acceleration measurements, due to the parameter associated with the strain–displacement transformation equation (i.e., α in Equation 15) which needs to be estimated. Park et al. used the bellow equation to estimate the unknown parameter:

$$\alpha = \sqrt{S_a(f_1)/S_s(f_1)}, \quad (21)$$

where S_a and S_s are the power spectral density (PSD) of the displacements estimated from strain measurements and the acceleration measured, respectively.²⁵ However, this technique has the following issues: (1) The parameter estimation is performed before displacement estimation, and hence, it is not applicable when the unknown parameter is time variant. (2) The performance of this technique highly relies on the accuracy of the identified first natural frequency.

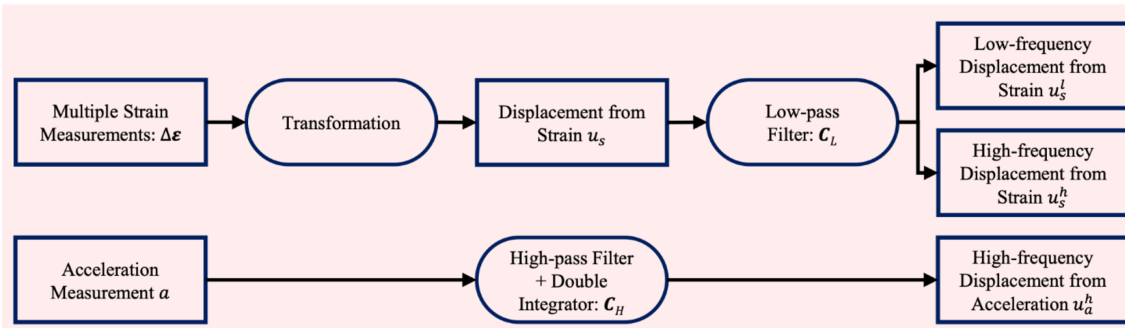
2.3 | Proposed displacement estimation technique by combining FIR filter and RLS algorithm

Figure 4 presents the flowchart of the proposed displacement estimation technique using strain and acceleration measured with the same sampling rate.

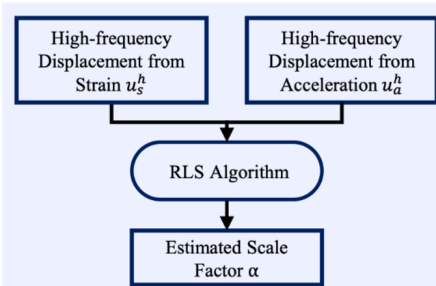
Step 1: the strain differences $\Delta\epsilon$ at multiple locations are transformed into the displacement, \mathbf{u}_s ,

$$\Delta\epsilon = \begin{bmatrix} \Delta\epsilon(x_1, k-N) & \cdots & \Delta\epsilon(x_1, k+N) \\ \vdots & \ddots & \vdots \\ \Delta\epsilon(x_m, k-N) & \cdots & \Delta\epsilon(x_m, k+N) \end{bmatrix}_{m \times (2N+1)}, \quad (22)$$

Step 1: FIR filter-based displacement estimation using strain and acceleration measurements, respectively



Step 2: Scale factor estimation



Step 3: Final displacement estimation

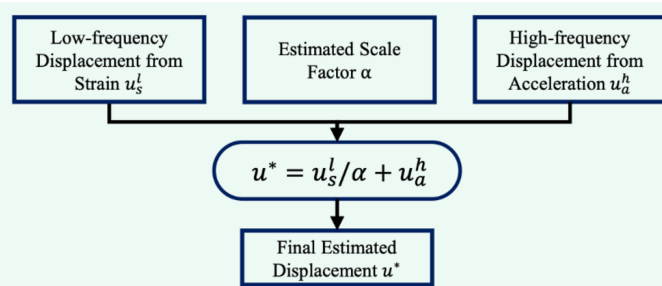


FIGURE 4 Flowchart of the proposed displacement estimation technique using strain and acceleration measured with same sampling frequency

$$\mathbf{u}_s = \{\mathbf{T}_a \mathbf{H}^{-1} \Delta \boldsymbol{\epsilon}\}^T, \quad (23)$$

$$\mathbf{u}_s = [u_s(k-N), u_s(k-N+1), \dots, u_s(k+N)]_{1 \times (2N+1)}^T. \quad (24)$$

Next, a low-pass filter, \mathbf{C}_L , is applied to the displacement, \mathbf{u}_s , and a combination of a high-pass filter and double integrator, \mathbf{C}_H , is applied to the acceleration measurement, \mathbf{a} :

$$\mathbf{a} = [a(k-N+1), a(k-N+2), \dots, a(k+N-1)]_{1 \times (2N-1)}^T. \quad (25)$$

Then, the low-frequency displacement from the strain measurements and the high-frequency displacement from the acceleration measurement are estimated as follows:

$$u_s^l(k) = \mathbf{C}_L \mathbf{u}_s, \quad (26)$$

$$u_a^h(k) = \mathbf{C}_H \mathbf{a}. \quad (27)$$

Additionally, the high-frequency displacement from the strain measurements is obtained as follows:

$$u_s^h(k) = u_s(k) - u_s^l(k). \quad (28)$$

Step 2: $\alpha(k)$ is used to scale $u_s^h(k)$ so that the amplitudes of u_a^h and u_s^h can be similar at each time step:

$$u_a^h(k) \approx \frac{1}{\alpha(k)} u_s^h(k). \quad (29)$$

Indeed, the value of $\alpha(k)$ is estimated using an RLS algorithm,²⁶

$$\alpha(k) = \alpha(k-1) + p(k) u_a^h(k) [u_s^h(k) - u_a^h(k) \alpha(k-1)], \quad (30)$$

$$p(k) = \frac{p(k-1)}{1 + p(k-1) [u_a^h(k)]^2}. \quad (31)$$

The estimated $\alpha(k)$ is then used to scale the low-frequency displacement from the strain gauges, $u_s^l(k)$, as well.

Step 3: the estimated displacement, $u^*(k)$, is obtained by combining scaled $u_s^l(k)$ and $u_a^h(k)$.

$$u^*(k) = \frac{1}{\alpha(k)} u_s^l(k) + u_a^h(k) = \frac{1}{\alpha(k)} \mathbf{C}_L \{\mathbf{T}_a \mathbf{H}^{-1} \Delta \boldsymbol{\epsilon}\}^T + \mathbf{C}_H \mathbf{a}. \quad (32)$$

Note that $u_a^h(k)$ is used instead of $\frac{1}{\alpha(k)} u_s^h(k)$ because an accelerometer typically has a higher signal-to-noise ratio (SNR) than that of a strain gauge, especially in the high-frequency range.

Typically, the sampling rate of the strain gauge is usually lower than that of the accelerometer. In such a case, the transformed displacement from strain measurements is up-sampled by cubic spline interpolation to match the sampling frequency to that of acceleration. Also, a fourth-order low-pass Butterworth filter with a cut-off frequency equal to Nyquist frequency of strain measurements is applied to $u_s^h(k)$ and $u_a^h(k)$ before the estimation of $\alpha(k)$.

An explanation describing how the fusion of strain and acceleration measurements improves the displacement estimation accuracy is provided here. First, displacement is estimated from acceleration measurement via double integration. Because the double integration amplifies the measurement error particularly in the low-frequency band, a high-pass filter is applied to suppress the low-frequency error. In fact, the proposed technique performs double

integration and high-pass filtering simultaneously using C_H . The issue here is that actual structural responses in the low-frequency range are also removed by the aforementioned high-pass filter. To recover the low-frequency structural responses, strain at multiple locations are measured and transformed into displacement. Then a low-pass filter, C_L , is applied to the strain-based displacement to retain only the low-frequency displacement. Finally, the low-frequency displacement from strain and the high-frequency displacement from acceleration are combined after scaling to produce the final displacement with improved accuracy.

3 | VALIDATION USING SIMPLY SUPPORTED BEAM MODEL

In this section, the proposed technique is validated by using a simply supported beam model subjected to three different excitations. Besides, the effect of number and locations of strain gauges on displacement estimation is investigated.

3.1 | Model description

A simply supported beam model with a uniform cross-section is simulated using SAP2000, as shown in Figure 5. The beam model has a length of 10 m and square cross-section of 120 mm × 120 mm. The strain gauges were placed at locations A, B, and C, while an accelerometer was placed only at location B, as shown in Figure 5a. Note that two strain gauges were installed at each cross-section as shown in Figure 5b.

Three different ground excitations are applied to the beam model, and the corresponding acceleration, strain, and displacement responses are computed. First, a random ground excitation with a frequency band of 0–50 Hz is applied (Excitation 1). Second, a combination of Excitation 1 and a low-frequency excitation below 0.1 Hz (Excitation 2) is applied. Third, the aforementioned low-frequency input without any random input is applied (Excitation 3). Note that Excitation 3 was obtained by taking the second derivative of a real bridge displacement with a scaling factor of 1/500. The three excitation signals are shown in Figure 6.

The displacement and acceleration responses at point B and the strain responses at points A, B, and C are all computed at a sampling rate of 100 Hz. Next, Gaussian noises are added to the acceleration and strain responses to simulate measurement noises. As accelerometers usually have higher SNRs than those of strain gauges, the SNR is set to 10 for strain responses and 20 for acceleration responses. The first natural frequency of this model is 1.75 Hz, so the time window size for the FIR filter is set to 153, according to Equation 18.

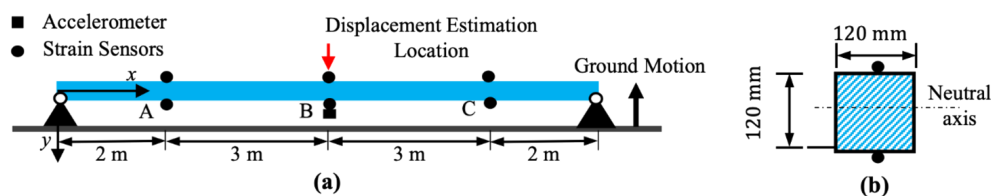


FIGURE 5 Uniform simply supported beam model: (a) dimensions and sensor layout, and (b) cross-section

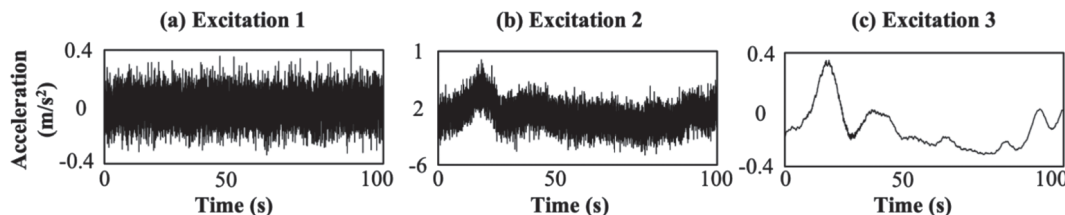


FIGURE 6 Three ground excitation signals applied to the simply supported beam: (a) Excitation 1, (b) Excitation 2, and (c) Excitation 3

3.2 | Displacement estimation results

Figure 7 presents the displacements estimated by the proposed technique and PSD technique.²⁵ In the case of Excitations 1 and 2, there is little difference between the displacements estimated by the two techniques as shown in Figure 7a,b. In the case of Excitation 3, the proposed technique estimates displacement more precisely than the PSD technique

The displacement estimation performance is compared in terms of the absolute peak value error (APVE) and normalized root mean square error (NRMSE) defined as follows:

$$\text{APVE} (\%) = 100 \left| \frac{\max(|u_e|) - \max(|u_r|)}{\max(|u_r|)} \right|, \quad (33)$$

$$\text{NRMSE} (\%) = 100 \sqrt{\frac{\sum (u_e - u_r)^2}{\sum (u_r)^2}}, \quad (34)$$

where u_r and u_e denote the reference and estimated displacements, respectively.

The comparison results are summarized in Table 1. For Excitations 1, 2, and 3, the proposed technique reduces the NRMSE by 1%, 24%, and 49%, respectively, compared to the PSD technique. The proposed technique also reduces APVE by 25% and 69% compared to the PSD technique for Excitations 1 and 3, respectively. On the other hand, an increase of 26% in APVE is observed for Excitation 2.

In practice, the first natural frequency obtained from acceleration measurements or FEM model, $f_{1,a}$, is used to approximate f_1 of a target structure. Here, the effect of the error in $f_{1,a}$ on displacement estimation accuracy is

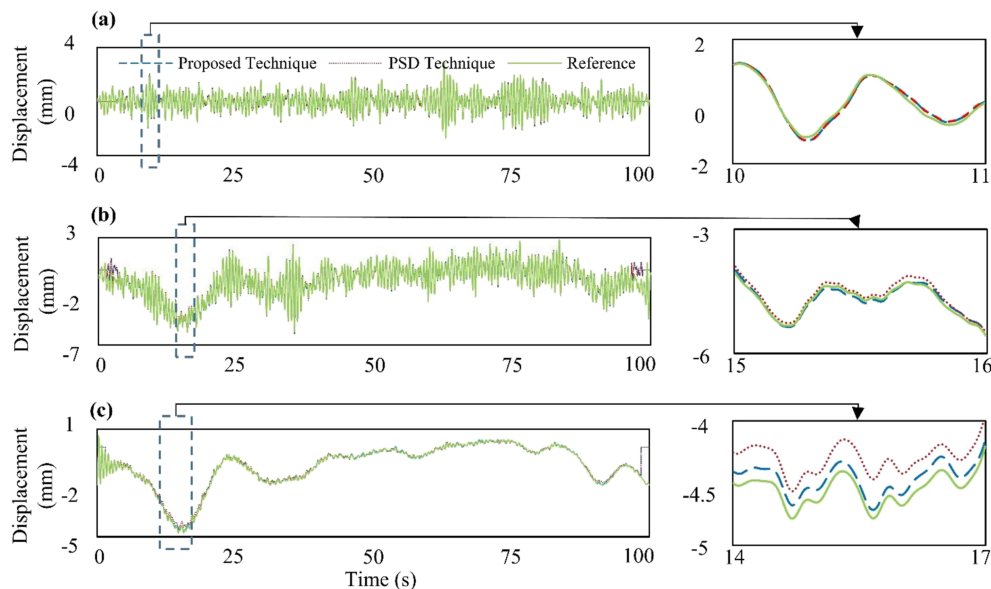


FIGURE 7 Displacements estimated by the proposed technique and PSD technique²⁵: (a) Excitation 1, (b) Excitation 2, and (3) Excitation 3

TABLE 1 Comparison of displacement estimation performance between the proposed technique and PSD technique

Excitations	Proposed technique		PSD technique	
	APVE (%)	NRMSE (%)	APVE (%)	NRMSE (%)
Excitation 1	2.77	12.92	3.71	13.03
Excitation 2	2.65	3.78	2.10	4.95
Excitation 3	1.45	2.74	4.62	5.79

investigated when the beam is subjected to Excitation 2. The results are shown in Table 2 considering $\pm 3\%$ difference between the actual natural frequency and the approximated one. The accuracy of the displacement estimated by the PSD technique highly relies on the accuracy of $f_{1,a}$, while that of the proposed technique is less sensitive to the accuracy of $f_{1,a}$.

3.3 | Effect of number and locations of strain gauges on displacement estimation

Here, the effects of the number of strain gauges and their locations on the displacement estimation accuracy are investigated when the simply supported beam is subjected to Excitation 2. The sensor layout is shown in Figure 8.

First, the effect of the number of strain gauges is studied. The number of strain gauges is increased from 1 to 9, and the corresponding displacement estimation errors are calculated, as shown in Table 3. Reductions of approximately 50% in both APVE and NRMSE values are observed when the strain gauge number increases from 1 to 3. Thereafter, increasing the number of strain gauges continues to yield a reduction in APVE but no significant improvement in NRMSE.

Next, the effect of the strain gauge locations is investigated using three strain gauges as shown in Table 4. In all cases, the NRMSE remains at around 4%, and the APVE is always below 3%.

4 | VALIDATION USING BEAM MODELS WITH VARYING CROSS-SECTION AND BOUNDARY CONDITIONS

In this section, a series of numerical simulation were conducted in SAP2000 to demonstrate that the use of the scale factor can effectively compensate for the discrepancies between the assumed and true mode shapes.

$f_{1,a}$ (Hz)	2N+1	Proposed technique		PSD technique	
		APVE (%)	NRMSE (%)	APVE (%)	NRMSE (%)
1.7 (0.97 f_1)	157	2.44	3.90	3.02	7.36
1.73 (0.99 f_1)	155	2.60	3.83	2.85	6.31
1.75 (f_1)	153	2.65	3.78	2.10	4.95
1.77 (1.01 f_1)	151	2.66	3.76	2.74	7.02
1.80 (1.03 f_1)	149	2.70	3.70	4.80	7.75

TABLE 2 The effect of error in the identified first natural frequency on displacement estimation accuracy

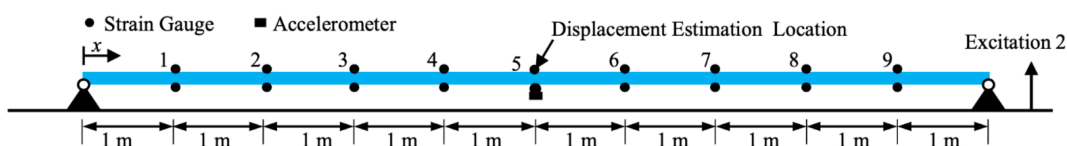


FIGURE 8 Sensor layout for investigating effect of number and locations of strain gauges on displacement estimation accuracy

# of strain gauges	Strain gauge locations	APVE (%)	NRMSE (%)
1	5	4.80	8.18
3	2, 5, 8	2.65	3.77
5	2, 4, 5, 6, 8	1.89	3.66
7	2, 3, 4, 5, 6, 7, 8	0.50	3.56
9	1, 2, 3, 4, 5, 6, 7, 8, 9	0.82	3.56

TABLE 3 Effect of number of strain gauges on displacement estimation accuracy

TABLE 4 Effect of strain gauge locations on displacement estimation accuracy

Strain gauge locations	APVE (%)	NRMSE (%)
1, 5, 9	0.55	3.93
2, 5, 8	2.65	3.77
3, 5, 7	1.55	3.72
4, 5, 6	0.42	3.98

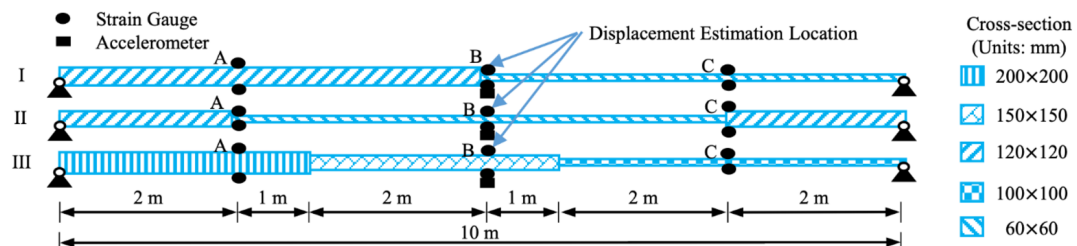


FIGURE 9 Three simply supported beam models with varying cross-sections

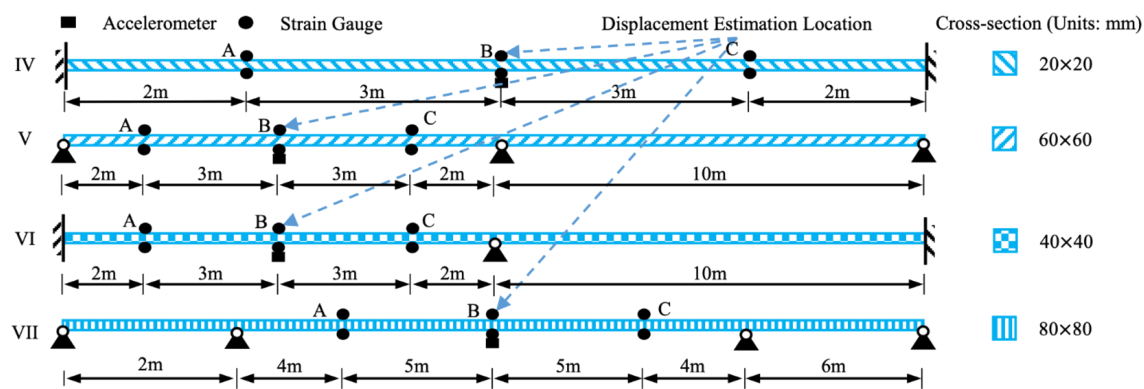


FIGURE 10 Four uniform cross-section beam models with different boundary conditions

4.1 | Model description

Three simply supported beam models with varying cross-sections, in addition to four uniform beam models with different cross-sections, spans, and boundary conditions, were created from previous simply supported beam model. The dimensions of the models and sensor layouts are shown in Figures 9 and 10. Strain gauges were placed at locations A, B, and C, while an accelerometer was placed only at location B, where the displacement needs to be estimated. Note that two strain gauges were placed on the top and bottom surfaces of beams for each of cross-sections of locations A–C. These beams were excited using Excitation 3 shown in Figure 6c. Time domain analyses were performed to compute the acceleration, strain, and displacement responses. All the simulated responses were sampled at 100 Hz. For multi-span beam models, it should be noted that the assumed mode shapes are applied only for the target span where the displacement needs to be estimated.

4.2 | Displacement estimation results

Owing to variations in cross-sections and boundary conditions, large discrepancies can exist between the assumed and true mode shapes for all seven models. An example is shown in Figure 11, where the first three mode shapes of model I are compared with the assumed mode shapes.

The effect of the scaling factor on displacement estimation are summarized in Table 5. Noise-free measurements are used here to clearly show the effect of the mode shape discrepancies on displacement estimation accuracy. Owing to the discrepancies between the assumed and true mode shapes, large errors are produced in the displacements estimated without using a scale factor. When the scale factor is employed to compensate for the errors, APVE and NRMSE are

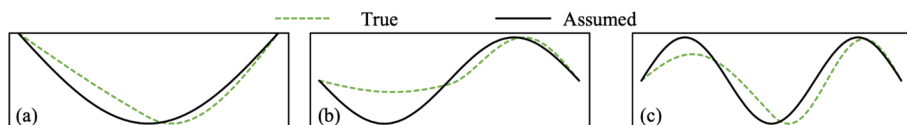


FIGURE 11 Comparison of true and assumed mode shapes of model I: (a) first mode shape, (b) second mode shape, and (c) third mode shape

TABLE 5 Accuracy comparison between the displacements estimated (1) without scale factor α , (2) with scale factor α , and (3) with scale factor α and measurement noises

Model #	(1) Without scale factor		(2) With scale factor		(3) With scale factor and measurement noises	
	APVE (%)	NRMSE (%)	APVE (%)	NRMSE (%)	APVE (%)	NRMSE (%)
I	40.56	46.75	0.57	0.74	1.02	1.69
II	24.17	25.63	1.10	1.54	1.56	2.04
III	18.43	5.61	0.15	0.15	0.76	2.69
IV	20.29	19.00	1.78	2.31	1.87	2.51
V	13.10	2.22	1.69	0.30	1.76	1.86
VI	19.86	4.73	1.56	0.65	1.74	2.4
VII	11.84	16.42	1.50	2.11	1.62	2.68

significantly reduced. However, the scale factor cannot fully remove the displacement estimation error even without any measurement noise in the strain gauges and the accelerometer.

Next, Gaussian white noises were added to the simulated responses, and the SNR values for strain and acceleration were set to 10 and 20, respectively. The APVE and NRMSE of the displacements estimated by proposed technique for all seven models are summarized in Table 5. Both APVE and NRMSE values are below 2% and 3%, respectively.

5 | VALIDATION USING JINDO GRAND BRIDGE MODEL

In this section, an FE model of the Jindo Grand Bridge in South Korea was built using SAP2000 to examine the performance of the proposed displacement estimation technique by extracting pure bending strain from strain measurements. Besides, the effect of estimation location on displacement estimation accuracy is investigated.

5.1 | Model description

The Jindo Grand Bridge in South Korea is a three-span cable-stayed bridge composed of one 344-m-long main span and two 70-m-long side spans. For simplicity, a beam model with a uniform circular cross-section and bending stiffness equivalent to that of the actual bridge cross-section is used. The strain gauges were placed at locations A, B, C, D, and E, as shown in Figure 12a, and two strain gauges at each cross-section were installed, as shown in Figure 12b. Eleven accelerometers were placed at locations 1–11, as shown in Figure 12a. As before, the acceleration, strain, and displacement responses are simulated when the model is subjected to Excitation 3, as shown in Figure 6c. The only difference is that the amplitude of Excitation 3 signal is scaled by 500 to generate a realistic displacement for this bridge model. As the first natural frequency of this bridge is 0.43 Hz, the size of the time window for the FIR filter was set to 623, in accordance with Equation 18.

5.2 | Displacement estimation results

First, the displacement is estimated at location C using the strain measurements at locations A–E and a single acceleration measurement at location C. The displacements estimated by the proposed technique and PSD technique are

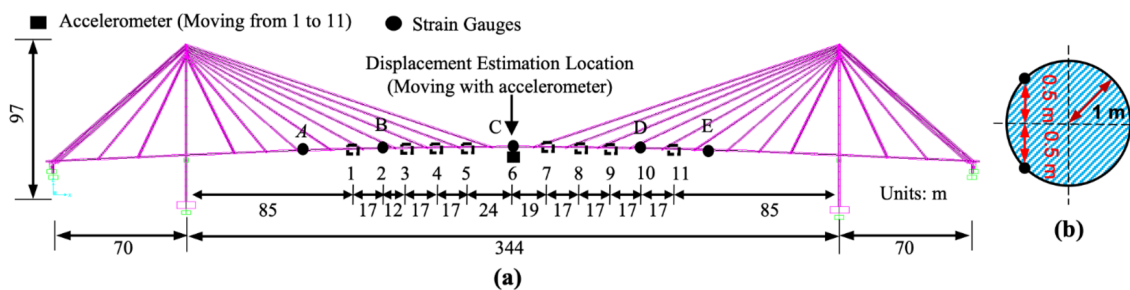


FIGURE 12 Overview of finite element model of Jindo grand bridge in South Korea: (a) dimensions and sensor layout, and (b) cross-section of beam model

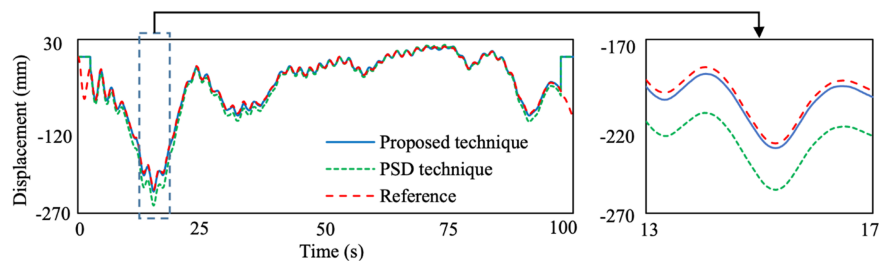


FIGURE 13 Displacements estimated using the proposed technique and PSD technique

TABLE 6 Comparison of displacement estimation accuracy

	Proposed technique	PSD technique
APVE (%)	1.90	7.60
NRMSE (%)	2.23	13.05

compared in Figure 13 and Table 6. Compared to the PSD technique, the proposed technique reduces the APVE and NRMSE to 15.53% and 16.17%, respectively. While strain measurements, which include uniform axial strain, are transformed into the displacement in the PSD technique, only pure bending strain, extracted from strain measurements, are transformed into displacement in the proposed technique.

Finally, the accelerometer is moved from location 1 to location 11 to estimate the displacement at those locations. The displacement estimation accuracy at those location is shown in Figure 14. While the APVE and NRMSE are below 2% and 3%, respectively, for locations 2–10, these errors increase rapidly at locations 1 and 11. As locations 1 and 11 are closer to the two supports than the other nine locations, the biggest discrepancy between the assumed and true mode shapes appears at these two locations. Therefore, the largest errors are observed at these two locations.

6 | EXPERIMENTAL VALIDATION

6.1 | Laboratory test on a fixed-fixed beam model

A laboratory test was performed to validate the performance of the proposed technique using an 830-mm-long fixed-fixed beam as shown in Figure 15. The beam consists of six steel elements, which are connected by bolts. The width and thickness of the beam are 30 and 1 mm, respectively, except for the connection part between two steel elements, the width and thickness of which are 70 and 2 mm, respectively. The dimensions of the steel elements are shown in Figure 15b. Young's module of the beam is 200 GPa. Two resistance-type strain gauges FLA-1-11-1LJC (Figure 15e) were installed on the top and bottom surfaces of the beam at locations A–C. Then, a triaxial MEMS accelerometer PCB-3713B112G (Figure 15d) was installed at location D, where the displacement needs to be estimated. The reference displacement was measured using a Polytech PSV-400-M4 laser Doppler vibrometer (LDV) (Figure 15c). The resolution of the LDV is 0.5 pm for displacement.²⁸ Two ends of the beam were fixed to a table using clamps.

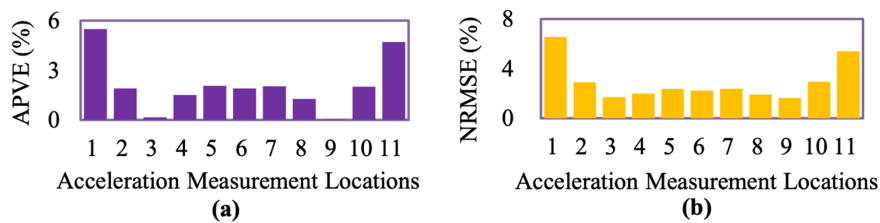


FIGURE 14 Comparison of displacement estimation accuracy at different locations: (a) APVE and (b) NRMSE

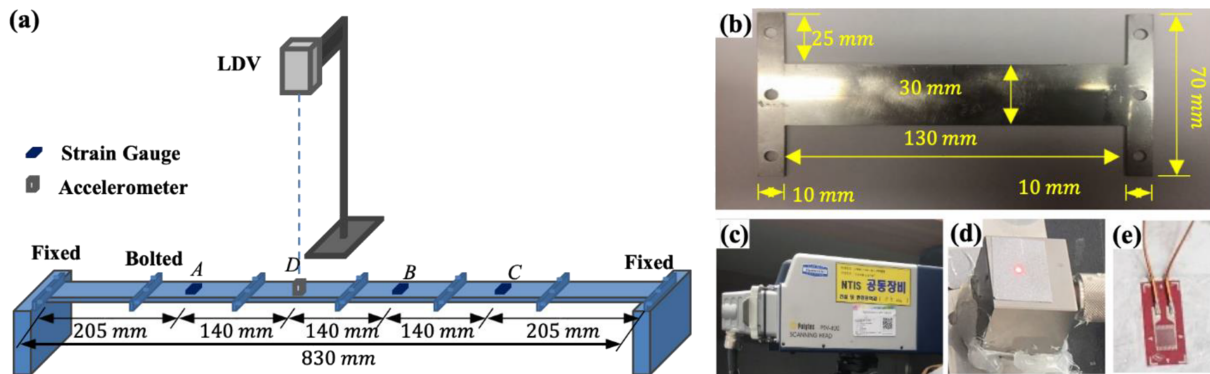


FIGURE 15 Experiment setup: (a) overview of the fixed–fixed beam and used sensors, (b) dimensions of steel element, (c) laser Doppler vibrometer (LDV) for reference displacement measurement, (d) accelerometer, and (e) strain gauge

The beam was manually excited by pushing and releasing the beam at multiple points. The sampling frequency of strain and acceleration measurement was set to 100 Hz. The first natural frequency identified from acceleration measurement is 7.8 Hz, so the time window size for the FIR filter is set to 35, according to Equation 18. The displacements at location D estimated by the proposed technique and PSD technique are shown in Figure 16, and the corresponding NRMSE and APVE are calculated in Table 7. Compared to the PSD technique, the proposed technique reduces RMSE and maximum error by 20% and 30%, respectively.

Next, the displacement is estimated by using strain and acceleration measured with different sampling frequencies. The sampling frequency of acceleration is fixed at 100 Hz while that of strain is decreased from 100 to 20 Hz. The displacement estimation accuracy is summarized in Figure 17. Both APVE and NRMSE increase with the decrease of the sampling frequency of strain measurements. Although the high-frequency component of strain measurements is not used for final displacement estimation, it is necessary for the estimation of scale factor α . The strain measurements with low sampling frequency fail to estimate the scale factor accurately and then cause a large error in the estimated displacement.

6.2 | Field test on a pedestrian bridge

The performance of the proposed technique was further validated using data obtained from a steel box-girder pedestrian bridge in Daejeon, Korea. The bridge is 45 m long and 8 m wide, and it has a uniform cross-section throughout its length. The experiment setup is shown in Figure 18. Three resistance-type strain gauges, FLA-5-11-1LJC, were installed at locations A, B, and C (1/4, 1/2, and 3/4 span points, respectively), and a uniaxial force balance accelerometer, EpiSensor ES-U2, was installed at location B, where the displacement was estimated. Strain data were wirelessly transmitted using three wireless sensor nodes, SG-link-200, and a wireless gateway, WSDA-200-USB. The reference displacement was measured using a Polytech RSV-150 laser Doppler vibrometer (LDV), which has a 0.3-nm resolution for displacement measurement.²⁹ All measurements were sampled at 128 Hz.

Figure 19 shows the recorded strain and acceleration responses at location B. For the first 0–33 s, the bridge was excited by jumping of four people on the bridge. For the second 33–50 s, the response was measured under free

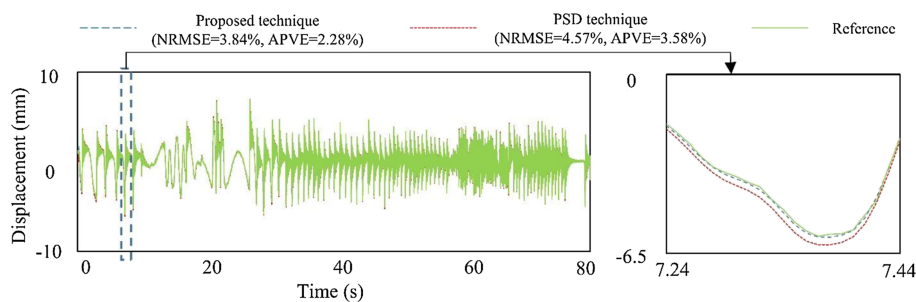


FIGURE 16 Displacements estimated using the proposed technique and PSD technique

TABLE 7 Comparison of displacement estimation accuracy

	Proposed technique	PSD technique
APVE (%)	2.28	3.28
NRMSE (%)	3.64	4.57

FIGURE 17 Effect of sampling frequency of strain measurements on displacement estimation accuracy

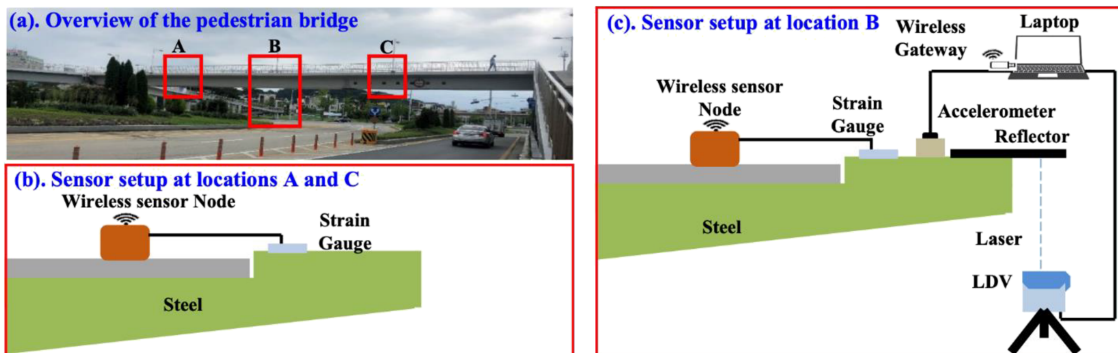
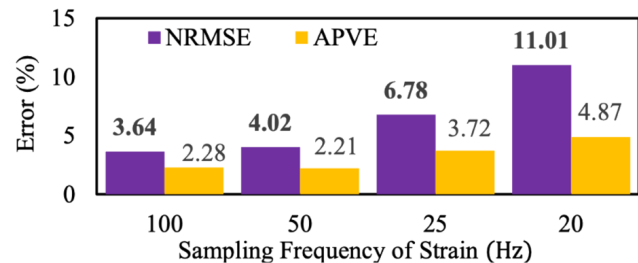


FIGURE 18 Experimental setup (a) overview of the pedestrian bridge, (b) strain gauge setup at locations A and C, and (c) strain gauge and accelerometer setup at location B

vibration. The first natural frequency identified from the acceleration measurement was 2.13 Hz, and the excitation frequency produced by jumping was 1.79 Hz.

The displacements of location B estimated by the proposed technique and PSD technique²⁵ are compared in Figure 20. The NRMSE errors of the proposed and PSD techniques are 10.28% and 12.04%, respectively. The proposed technique reduces NRMSE by 14.62% compared to the PSD technique. Although the NRMSE is larger than 10% for both techniques, the maximum error is only 0.32 and 0.40 mm for the proposed technique and PSD technique, respectively, as shown in Figure 21. Because the bridge has a strong high-frequency vibration, displacements are mainly estimated from acceleration measurement for both techniques. However, the difference between two techniques lies in the displacement estimated from strain measurements, and only a slight improvement was achieved by the proposed technique compared to the PSD technique.

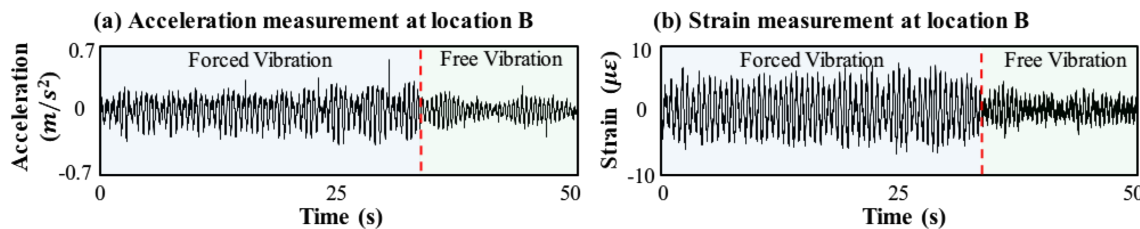


FIGURE 19 Measurements: (a) acceleration, and (b) strain at location B

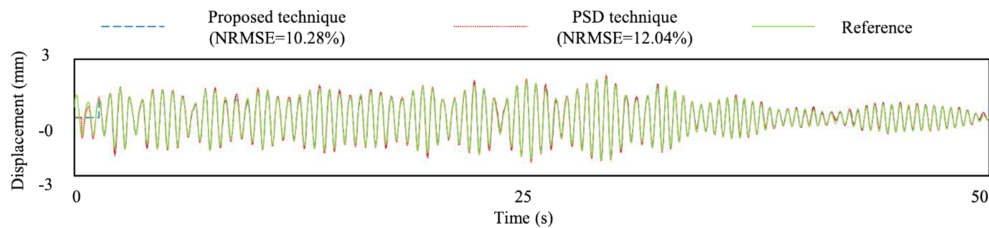


FIGURE 20 Displacements estimated by the proposed technique and PSD technique

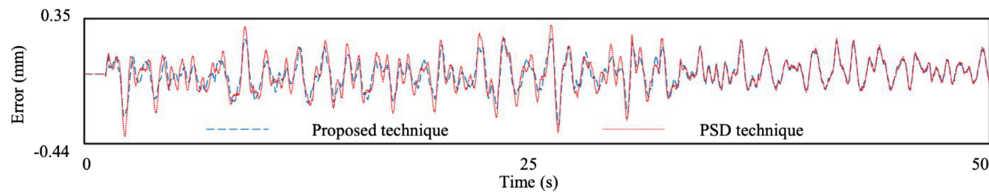


FIGURE 21 Displacement estimation errors of the proposed technique and PSD technique

7 | CONCLUSIONS

In this study, a new displacement estimation technique for bridge structures is proposed by fusing acceleration measurement from a single location and strain measurements from multiple locations. The performance of the proposed displacement estimation technique was firstly validated through numerical simulations of beams with varying cross-sections and boundary conditions and cable-stayed bridge models. The APVE and NRMSE of the estimated displacement were less than 2% and 3%, respectively, for all the numerical simulations investigated in this study. Next, the proposed technique was validated through a laboratory test using a fixed-fixed beam model, and the APVE and NRMSE of the estimated displacement were equal to 2.28% and 3.64%, respectively. In addition, a field test was conducted on a pedestrian bridge, and the maximum displacement error using the proposed technique was 0.32 mm. The validation tests performed showed that the proposed technique can accurately estimate both low-frequency and high-frequency displacements even with the discrepancy between the true and assumed mode shapes. Although the discrepancy between the true and assumed mode shapes are partially compensated by the proposed technique, the applicability of the proposed technique is inherently limited only to beam-like structures. Future work will focus on examining the applicability of the proposed technique to other types of structures with the help of FEM modeling. In such a case, the model shapes obtained from a FEM model can be used as the assumed mode shapes, improving the displacement estimation accuracy.

ACKNOWLEDGMENTS

This work was supported by the National Research Foundation of Korea (NRF) grant funded by the Korea government (MSIT) (No. 2017R1A5A1014883). The authors also thank Professor Soojin Cho at the University of Seoul and Professor Hongki Jo at the University of Arizona for providing the FE model of the Jindo Grande Bridge in South Korea and students from Smart Structures and Systems Lab in KAIST for their assistance during the field test.

ORCID

Hoon Sohn <https://orcid.org/0000-0001-9337-6653>

REFERENCES

1. Feng D, Feng MQ. Output-only damage detection using vehicle-induced displacement response and mode shape curvature index. *Struct Control Health Monit.* 2016;23(8):1088-1107.
2. Feng D, Feng MQ. Model updating of railway bridge using in situ dynamic displacement measurement under trainloads. *J Bridge Eng.* 2015;20(12):4015019.
3. Sun Z, Nagayama T, Nishio M, Fujino Y. Investigation on a curvature-based damage detection method using displacement under moving vehicle. *Struct Control Health Monit.* 2018;25(1):e2044.
4. Moreu F, Jo H, Li J, et al. Dynamic assessment of timber railroad bridges using displacements. *J Bridge Eng.* 2014;20(10):4014114.
5. Joshi S, Harle S. Linear variable differential transducer (LVDT) & its applications in civil engineering. *Int J Transp Eng Technol.* 2017; 3(4):62-66.
6. Nassif HH, Gindy M, Davis J. Comparison of laser Doppler vibrometer with contact sensors for monitoring bridge deflection and vibration. *Ndt & E International.* 2005;38(3):213-218.
7. Gentile C, Bernardini G. An interferometric radar for non-contact measurement of deflections on civil engineering structures: laboratory and full-scale tests. *Struct Infrastruct Eng.* 2010;6(5):521-534.
8. S N. GPS measurement of wind-induced suspension bridge girder displacements. *J Struct Eng.* 2000;126(12):1413-1419.
9. Cigada A, Mazzoleni P, Zappa E. Vibration monitoring of multiple bridge points by means of a unique vision-based measuring system. *Exp Mech.* 2014;54(2):255-271.
10. Fukuda Y, Feng MQ, Shinozuka M. Cost-effective vision-based system for monitoring dynamic response of civil engineering structures. *Struct Control Health Monit.* 2010;17(8):918-936.
11. Lee HS, Hong YH, Park HW. Design of an FIR filter for the displacement reconstruction using measured acceleration in low-frequency dominant structures. *Int J Numer Methods Eng.* 2010;82(4):403-434.
12. Gomez F, Park J-W, Spencer BF Jr. Reference-free structural dynamic displacement estimation method. *Struct Control Health Monit.* 2018;25(8):e2209.
13. Boore DM. *Effect of baseline corrections on response spectra for two recordings of the 1999 Chi-Chi, Taiwan, earthquake.* US Department of the Interior, US Geological Survey; 1999.
14. Boore DM. Effect of baseline corrections on displacements and response spectra for several recordings of the 1999 Chi-Chi, Taiwan, earthquake. *Bull Seismol Soc Am.* 2001;91(5):1199-1211.
15. Shin S, Lee S-U, Kim Y, Kim N-S. Estimation of bridge displacement responses using FBG sensors and theoretical mode shapes. *Struct Engng Mech.* 2012;42(2):229-245.
16. Wang Z, Geng D, Ren W, Liu H. Strain modes based dynamic displacement estimation of beam structures with strain sensors. *Smart Mater Struct.* 2014;23(12):125045.
17. Xia Y, Zhang P, Ni Y, Zhu H. Deformation monitoring of a super-tall structure using real-time strain data. *Eng Struct.* 2014;67:29-38.
18. Shen S, Wu Z, Yang C, Wan C, Tang Y, Wu G. An improved conjugated beam method for deformation monitoring with a distributed sensitive fiber optic sensor. *Struct Health Monit.* 2010;9(4):361-378.
19. Zhang Q, Zhang J, Duan W, Wu Z. Deflection distribution estimation of tied-arch bridges using long-gauge strain measurements. *Struct Control Health Monit.* 2018;25(3):e2119.
20. Helmi K, Taylor T, Zarafshan A, Ansari F. Reference free method for real time monitoring of bridge deflections. *Eng Struct.* 2015;103: 116-124.
21. Kim K, Jaemook C, Koo G, Sohn H. Dynamic displacement estimation by fusing biased high-sampling rate acceleration and low-sampling rate displacement measurements using two-stage Kalman estimator. *Smart Struct Syst.* 2016;17(4):647-667.
22. Casciati F, Casciati S, Vece M. Validation range for KF data fusion devices. *Acta Mech.* 2018;229(2):707-717.
23. Kim J, Kim K, Sohn H. Autonomous dynamic displacement estimation from data fusion of acceleration and intermittent displacement measurements. *Mech Syst Signal Process.* 2014;42(1):194-205.
24. Park J-W, Moon D-S, Yoon H, Gomez F, Spencer BF Jr, Kim JR. Visual-inertial displacement sensing using data fusion of vision-based displacement with acceleration. *Struct Control Health Monit.* 2018;25(3):e2122.
25. Park J-W, Sim S-H, Jung H-J. Displacement estimation using multimetric data fusion. *IEEE/ASME Trans Mechatr.* 2013;18(6): 1675-1682.
26. Haykin S. *Adaptive Filter Theory.* Pearson Education India; 2005.
27. Soman R, Ostachowicz W. Kalman Filter based Neutral Axis tracking for damage detection in composites structures under changing axial loading conditions. *Compos Struct.* 2018;206:517-525.
28. RSV-400 Scanning Vibrometer Datasheet, Polytech GmbH; 2005.
29. RSV-150 Remote Sensing Vibrometer Datasheet, Polytech GmbH; 2014.

How to cite this article: Ma Z, Chung J, Liu P, Sohn H. Bridge displacement estimation by fusing accelerometer and strain gauge measurements. *Struct Control Health Monit.* 2021;28:e2733. <https://doi.org/10.1002/stc.2733>

APPENDIX A: DERIVATION OF ERROR FUNCTION Π_E

When acceleration measurement is available, an error function $\Pi_E(u^*(t))$ is defined within a given time window $[T_1, T_2]$ as follows¹¹:

$$\Pi_E(u^*(t)) = \frac{1}{2} \int_{T_1}^{T_2} \left(\frac{d^2 u^*(t)}{dt^2} - a(t) \right)^2 dt, \quad (\text{A1})$$

where u^* and a are the estimated displacement at the final stage and the measured acceleration, respectively. As \bar{a} is measured with a constant time increment Δt , Equation A1 can be discretized using the trapezoidal rule with an odd number of time steps:

$$\begin{aligned} \Pi_E(u^*(k)) = & \frac{1}{2} \left(\frac{1}{2} \{a_u(k-N+1) - a(k-N+1)\}^2 + \{a_u(k-N+2) - a(k-N+2)\}^2 \right. \\ & \left. + \cdots + \{a_u(k+N-2) - a(k+N-2)\}^2 + \frac{1}{2} \{a_u(k+N-1) - a(k+N-1)\}^2 \right), \end{aligned} \quad (\text{A2})$$

where $a_u(k)$ is the approximation of the second-order differential of $u^*(t)$ at k th time step and is calculated by the following central difference method:

$$\frac{d^2 u^*(t)}{dt^2} \Big|_{t=k\Delta t} \approx a_u(k) = \frac{u^*(k+1) - 2u^*(k) + u^*(k-1)}{(\Delta t)^2}. \quad (\text{A3})$$

Introducing Equation A3 to Equation A2, Π_E can be rewritten in a matrix form

$$\Pi_E(\mathbf{u}^*) = \frac{1}{2} \left(\frac{1}{(\Delta t)^2} \mathbf{L}_c \mathbf{u}^* - \bar{\mathbf{a}} \right)^T \mathbf{L}_a^T \mathbf{L}_a \left(\frac{1}{(\Delta t)^2} \mathbf{L}_c \mathbf{u}^* - \bar{\mathbf{a}} \right) = \frac{1}{2} \frac{1}{(\Delta t)^4} \|\mathbf{L}_a \mathbf{L}_c \mathbf{u}^* - (\Delta t)^2 \mathbf{L}_a \bar{\mathbf{a}}\|_2^2, \quad (\text{A4})$$

where \mathbf{u}^* and \mathbf{a} are the final displacement estimation vector $[u^*(k-N), u^*(k-N+1), \dots, u^*(k+N)]^T$ and measured acceleration vector $[a(k-N+1), a(k-N+2), \dots, a(k+N-1)]^T$. \mathbf{L}_c and \mathbf{L}_a are defined as follows:

$$\mathbf{L}_c = \begin{bmatrix} 1 & -2 & 1 & & & \\ & 1 & -2 & 1 & & \\ & & \ddots & \ddots & \ddots & \\ & & & 1 & -2 & 1 \\ & & & & 1 & -2 & 1 \end{bmatrix}, \mathbf{L}_a = \begin{bmatrix} \frac{1}{\sqrt{2}} & & & & & \\ & 1 & & & & \\ & & \ddots & & & \\ & & & 1 & & \\ & & & & \frac{1}{\sqrt{2}} & \end{bmatrix}, \quad (\text{A5})$$

where the dimensions of \mathbf{L}_c and \mathbf{L}_a are $(2N-1) \times (2N+1)$, and $(2N-1) \times (2N-1)$, respectively. By minimizing Equation A4 with respect to \mathbf{u}^* , the final estimated displacement can be estimated as follows:

$$\mathbf{u}^* = (\Delta t)^2 (\mathbf{L}^T \mathbf{L})^{-1} \mathbf{L}^T \mathbf{L}_a \mathbf{a}, \quad (\text{A6})$$

where $\mathbf{L} = \mathbf{L}_a \mathbf{L}_c$. However, Equation A6 fails to yield a unique solution owing to the rank deficiency of \mathbf{L}_c . Provided that the displacement estimated from strain measurements is available, Π_E can be rewritten

$$\Pi_E(\mathbf{u}^*) = \frac{1}{2} \|\mathbf{L}_a \mathbf{L}_c \mathbf{u}^* - (\Delta t)^2 \mathbf{L}_a \mathbf{a}\|_2^2 + \frac{\lambda^2}{2} \|\mathbf{u}^* - \mathbf{u}\|_2^2, \quad (\text{A7})$$

where \mathbf{u} is the vector of the displacement transformed from strain measurements $[u(k-N), u(k-N+1), \dots, u(k+N)]^T$ and λ is the regularization factor. By minimizing Equation A7 with respect to \mathbf{u}^* , the final estimated displacement can be obtained as follows:

$$\mathbf{u}^* = (\Delta t)^2 (\mathbf{L}^T \mathbf{L} + \lambda^2 \mathbf{I})^{-1} \mathbf{L}^T \mathbf{L}_a \mathbf{a} + \lambda^2 (\mathbf{L}^T \mathbf{L} + \lambda^2 \mathbf{I})^{-1} \mathbf{u}. \quad (\text{A8})$$